View metadata, citation and similar papers at core.ac.uk
brought to you by CORE
provided by CERN Document Server

ALEPH 99-065
CONF 99-039
EPS-HEP99
Abstract #5_393
Parallel session: 5
Plenary session: 5
30 June 1999

OPEN-99-259
15/10/99

P R E L I M I N A R Y

Leptonic decays of the D_s meson

The ALEPH Collaboration

Abstract

The purely leptonic decays $D_s \to \tau\nu$ and $D_s \to \mu\nu$ are studied in a sample of four million hadronic Z decays collected with the ALEPH detector at LEP. The branching fractions are measured to be

$$\begin{aligned} B(D_s \to \tau\nu) &= [4.9 \pm 0.9(\text{stat}) \pm 1.6(\text{syst}) \pm 1.4(\text{BR})]\% \\ B(D_s \to \mu\nu) &= [0.64 \pm 0.08(\text{stat}) \pm 0.21(\text{syst}) \pm 0.15(\text{BR})]\% \ , \end{aligned}$$

where the last error in each case is due to the uncertainty on $B(D_s \to \phi\pi)$. Within the Standard Model, the results correspond to

$$f_{D_s} = [261 \pm 20(\text{stat}) \pm 43(\text{syst}) \pm 35(\text{BR})]\,\text{MeV} \ .$$

ALEPH contribution to 1999 summer conferences
Contact person: Harry He (he@phys.washington.edu)

1 Introduction

The branching fraction of the D_s to a lepton and a neutrino is interesting because in the quark model it represents the annihilation of the D_s meson's constituent quark and antiquark. The rate of these decays is governed partly by the quark-antiquark wavefunction at the origin. This quantity is parametrized by the D_s decay constant f_{D_s}. Besides its own intrinsic interest this measurement is useful because it sheds light on the theoretical understanding of the decay constants of other heavy mesons. The B and B_s meson decay constants influence the B-$\bar{B}$ mixing rates. At present these decay constants cannot be measured experimentally, so the interpretation of mixing measurements depends on theoretical calculations. Better experimental determination of f_{D_s} will serve as a valuable check on these calculational techniques. Knowing the values of f_B and f_{B_s} will allow for the extraction of the third generation CKM matrix elements from the B mixing measurements and further constrain the three-generation mixing unitarity triangle.

Preliminary measurements of $B(D_s \to \tau\nu)$ and $B(D_s \to \mu\nu)$ are presented in this paper. The analyses are based on a sample of 3.97 million produced hadronic Z decays collected in 1991–1995 with the ALEPH detector at LEP. The branching fraction for the leptonic decay $D_s \to \ell\nu$ is given in the Standard Model by

$$B(D_s \to \ell\nu) = \tau_{D_s} \frac{G_{\mathrm{F}}^2}{8\pi} f_{D_s}^2 |V_{cs}|^2 M_{D_s} M_\ell^2 \left(1 - \frac{M_\ell^2}{M_{D_s}^2}\right)^2, \qquad (1)$$

where τ_{D_s} is the lifetime of the D_s meson, G_{F} is the Fermi coupling constant, V_{cs} is a CKM matrix element, and M_ℓ and M_{D_s} are the lepton and D_s masses. This relation is used to extract the value of f_{D_s} from the measured branching fractions.

2 $D_s \to \tau\nu$ analysis

2.1 Event selection

In this analysis, we search for the decay chain

$$e^+e^- \to c\bar{c}, \;\; c \to D_s, \;\; D_s \to \tau\nu, \;\; \tau \to e\bar{\nu}_e\nu_\tau \;\text{ or }\; \tau \to \mu\bar{\nu}_\mu\nu_\tau.$$

Because electrons and muons are identified with different techniques, the electron and muon channels are treated separately. As the final state under study contains three neutrinos, the signature of these decays is an identified lepton and large missing energy in one hemisphere of the event.

Hadronic Z decays are preselected with the standard ALEPH selections based on charged tracks. The $e^+e^- \to \ell^+\ell^-$ and $e^+e^- \to \gamma\gamma$ events are rejected by cutting on the number of reconstructed charged tracks. The event thrust axis is required to satisfy $|\cos\theta_{\mathrm{thrust}}| < 0.8$ to select events within the acceptance of the vertex detector. Each event is then separated into two hemispheres with the plane perpendicular to the thrust axis. The total energy of each hemisphere is calculated and the one with larger missing energy is selected if there is an identified lepton (e or μ) in that hemisphere. Electron identification is based on the shower shape in the electromagnetic calorimeter and the

ionization in the time projection chamber; muon identification makes use of the digital pattern information in the hadron calorimeter and hits in the muon chambers [1]. The missing energy in the hemisphere is required to be greater than 5 GeV to reduce the background. The hemisphere invariant masses are taken into account in the calculation of the expected energies.

To further reduce the background from $b\bar{b}$ events, cuts are applied to a set of hemisphere variables based on the rapidities and impact parameters of the charged tracks. An existing ALEPH lifetime tag [2] was modified to include a dependence on the rapidity of the charged tracks with respect to the nearest jet axis. Events from $c\bar{c}$ are expected to have higher rapidity tracks than $b\bar{b}$ events because of the lower mass of c hadrons compared to b hadrons. Additionally, if one excludes the identified lepton, signal events will only have fragmentation tracks in the lepton hemisphere and can be distinguished from $c\bar{c}$ background events. The tracks in each hemisphere are divided according to whether their rapidities are greater than or less than a certain value. The confidence levels that the sets of high and low rapidity tracks in each hemisphere originate from the Z production point are then calculated. Cuts are made on the confidence level for the low rapidity tracks in each hemisphere, and on the high rapidity tracks' confidence level in the hemisphere containing the selected lepton.

The momentum and energy of the D_s candidate are reconstructed from the observed charged and neutral particles in the event by excluding the lepton and applying four-momentum conservation:

$$\begin{aligned} \vec{P}_{D_s} &= -\sum_{i \neq \text{lepton}} \vec{P}_i \\ E_{D_s} &= \sqrt{s} - \sum_{i \neq \text{lepton}} E_i. \end{aligned}$$

A kinematic fit is performed in which the energies of all reconstructed particles (except the lepton) are varied such that the constraint $[E_{D_s}^2 - P_{D_s}^2]^{1/2} = M_{D_s} = 1.968\,\text{GeV}/c^2$ is satisfied. The energy resolutions for charged, neutral electromagnetic, and neutral hadronic objects are parametrized from simulated events. The kinematic fit improves the energy resolution of D_s candidates from 6.7 GeV to 3.5 GeV. The background is further reduced by the requirement that the fitted E_{D_s} be greater than 25 GeV. The selection efficiency for $c\bar{c} \to D_s \to \tau\nu$ events is 2.2% (2.9%) in the electron (muon) channel [including the factor of $B(\tau \to \ell\nu\bar{\nu})$].

A linear discriminant analysis is performed on Monte Carlo events to search for an optimal linear combination of variables so that maximum discrimination between signal and background is achieved. Two discriminating variables U_c and U_b are created to distinguish the $c\bar{c} \to D_s \to \tau\nu$ signal events from $c\bar{c}$ and $b\bar{b}$ backgrounds, respectively. The input variables with the greatest discrimination power include the fitted D_s momentum, the angle between the lepton and the D_s direction (boosted to the D_s rest frame), several b tag variables, and the total momentum of the reconstructed particles in the lepton hemisphere. The definitions of U_c and U_b are optimized independently in the electron and muon channels. The distributions of U_c and U_b are shown in Figs. 1 and 2.

The branching fraction $B(D_s \to \tau\nu)$ is extracted from a two-dimensional unbinned maximum likelihood fit to the U_b vs U_c distribution in each channel. The fitting function consists of one signal and three background (uds, $c\bar{c}$, and $b\bar{b}$) components. The signal

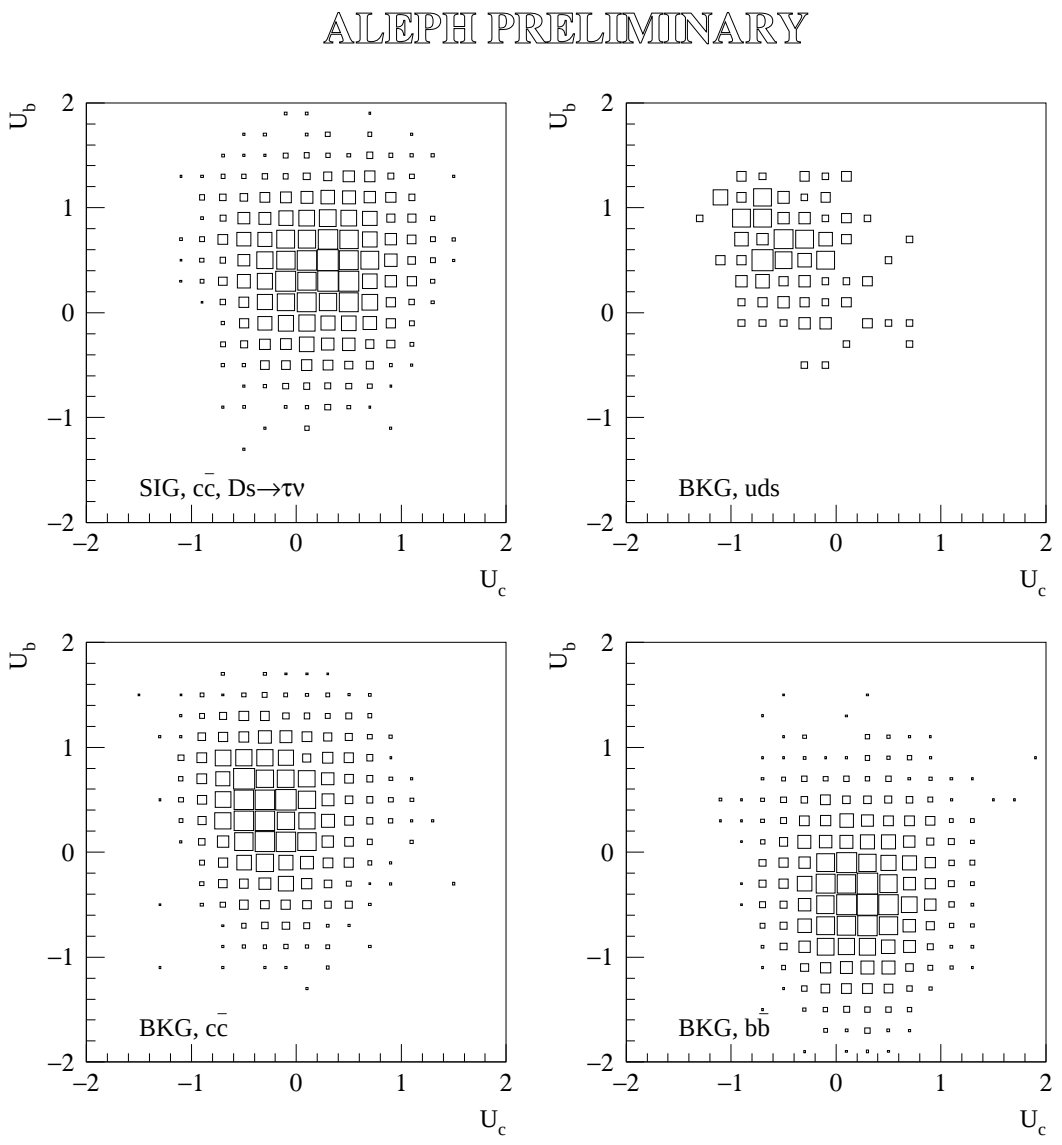

Figure 1: $D_s \to \tau\nu$ analysis: unnormalized Monte Carlo U_b vs U_c distributions for the signal and the three backgrounds in the electron channel.

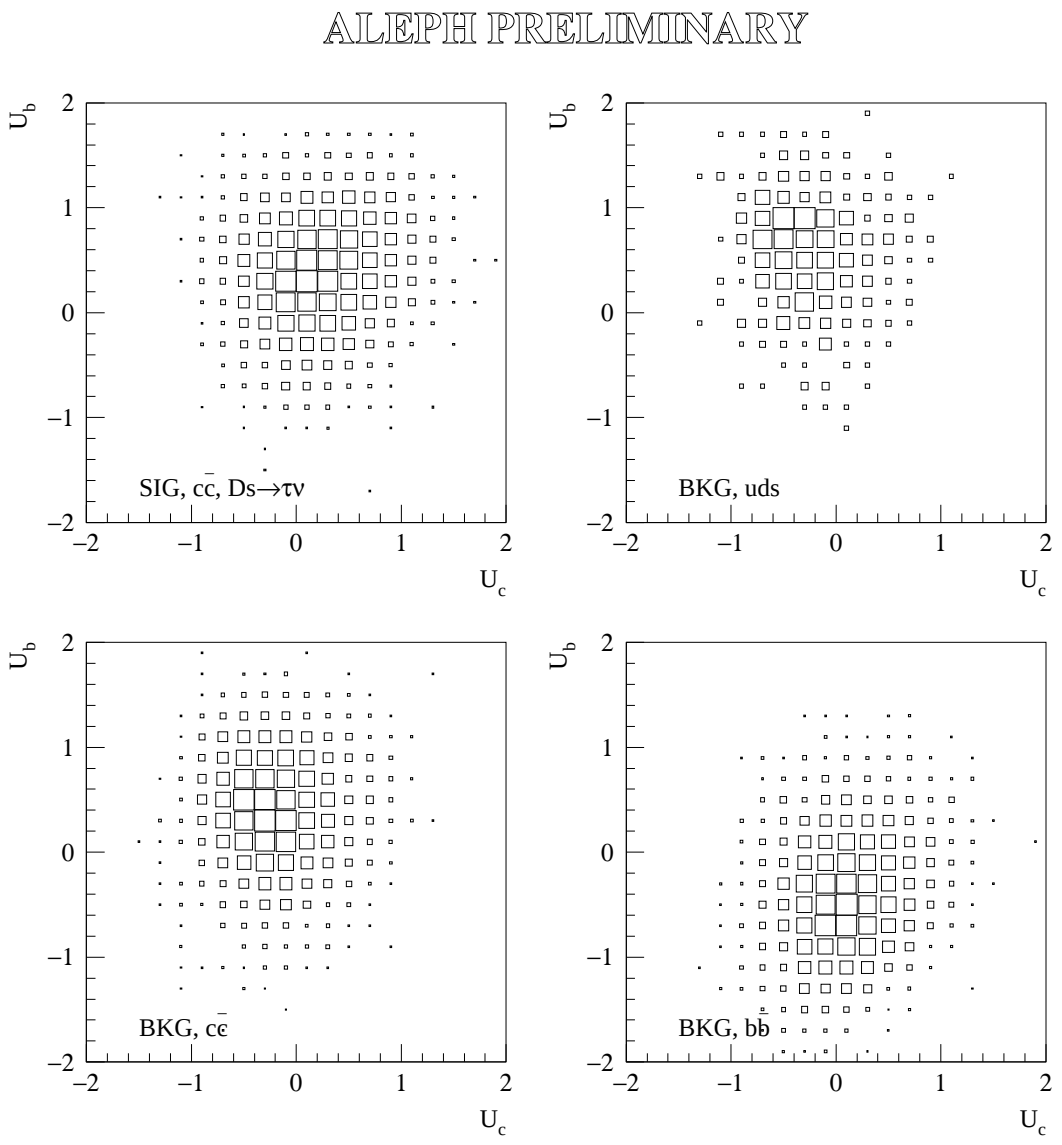

Figure 2: $D_s \to \tau\nu$ analysis: unnormalized Monte Carlo U_b vs U_c distributions for the signal and the three backgrounds in the muon channel.

Table 1: Fitted numbers of events in the $D_s \to \tau\nu$ analysis. The relative normalizations of the various signal contributions are fixed as described in the text.

	Number of Events	
Source	e channel	μ channel
Background		
uds	123	496
$c\bar{c}$	1386	2236
$b\bar{b}$	1729	2616
Total	3238	5348
Signal		
$c\bar{c} \to D_s \to \tau\nu$	151	199
$b\bar{b} \to D_s \to \tau\nu$	59	70
$c\bar{c} \to D_s \to \mu\nu$	1	103
$b\bar{b} \to D_s \to \mu\nu$	4	21
$D^+ \to \ell\nu$	10	34
Total	225	427

component is the combination of D_s and D^+ decays to $\tau\nu$ and $\mu\nu$ in $c\bar{c}$ and $b\bar{b}$ events. The relative normalizations of these eight contributions are fixed according to Eq. 1 and the measured charm production rates [3–5], $f_{D_s}/f_D = 1.10 \pm 0.06$ from lattice QCD predictions [6], and other quantities from [7]. Leptonic D^+ decays are Cabibbo suppressed and contribute less than 8% of the total signal. Each component of the fitting function is parametrized as the sum of up to five two-dimensional correlated Gaussian functions from a fit to simulated events. The free parameters in the fit to the data are the numbers of events in the signal and the three background components. The fitting procedure is tested with Monte Carlo events to be free of biases.

2.2 Results of the $D_s \to \tau\nu$ analysis

The projections of the two-dimensional fits to the data are shown in Fig. 3. The fitting functions are found to yield a good description of the U_b vs U_c distributions in data: the fit confidence level is 94% in the electron channel and 67% in the muon channel.

The same projections are shown in Figs. 4 and 5 after subtraction of the fitted background components. The distribution of the excess events is consistent in shape with the Monte Carlo prediction for the signal.

The fitted branching fractions from the electron and muon channels are $B(D_s \to \tau\nu) = [4.93 \pm 1.43(\text{stat})]\%$ and $[4.87 \pm 0.93(\text{stat})]\%$, respectively. The contribution of each component is shown in Table 1.

2.3 Systematic uncertainties

The systematic uncertainties in the two channels are listed in Table 2.

The Monte Carlo events used to parametrize the fitting functions are reweighted to

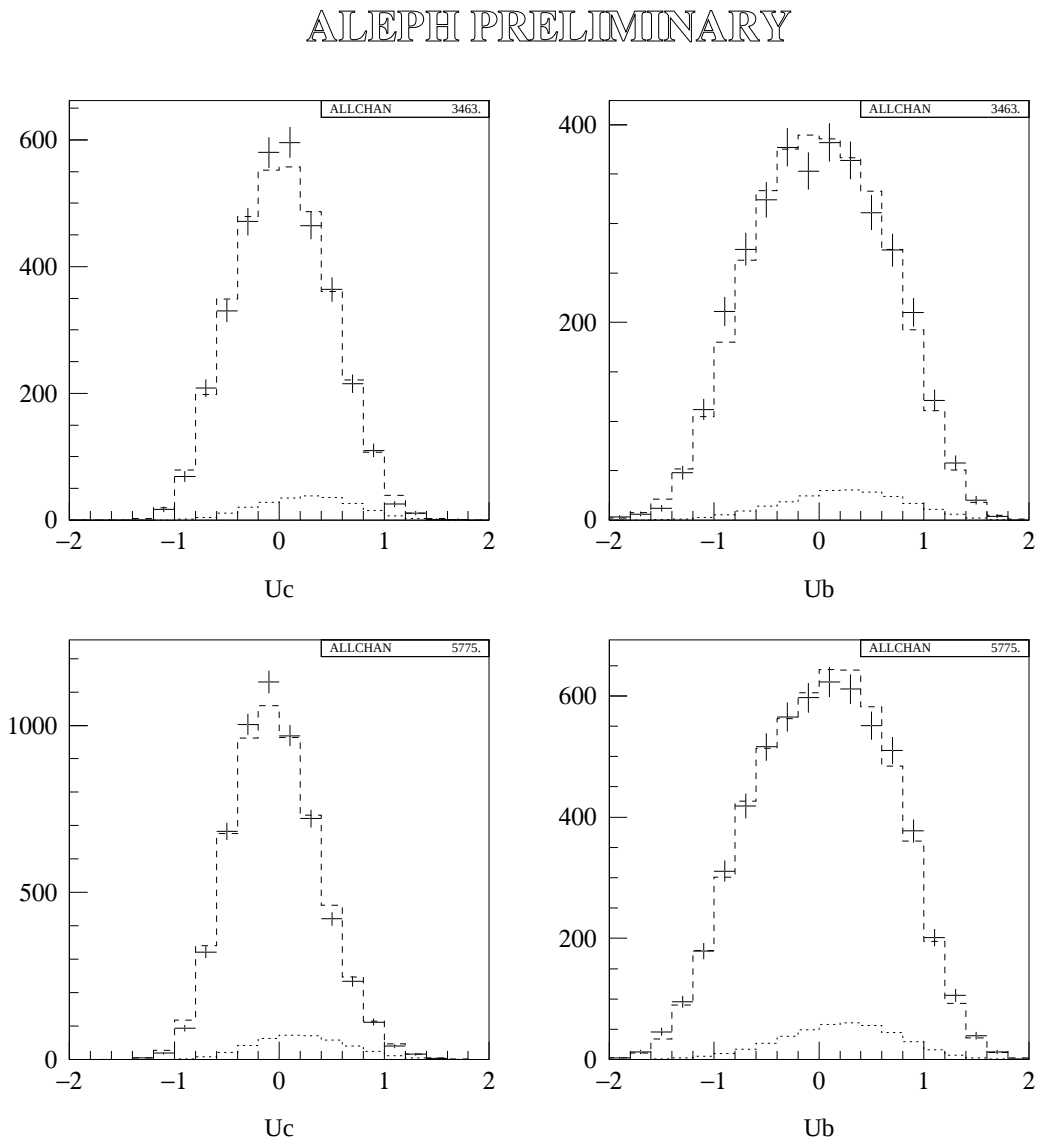

Figure 3: $D_s \to \tau\nu$ analysis: projections of the two-dimensional fits to the data. The crosses show the data distributions, while the dashed histograms are the fit results. The dotted histograms show the fitted signal contributions. The upper two plots are for the electron channel and the lower two for the muon channel.

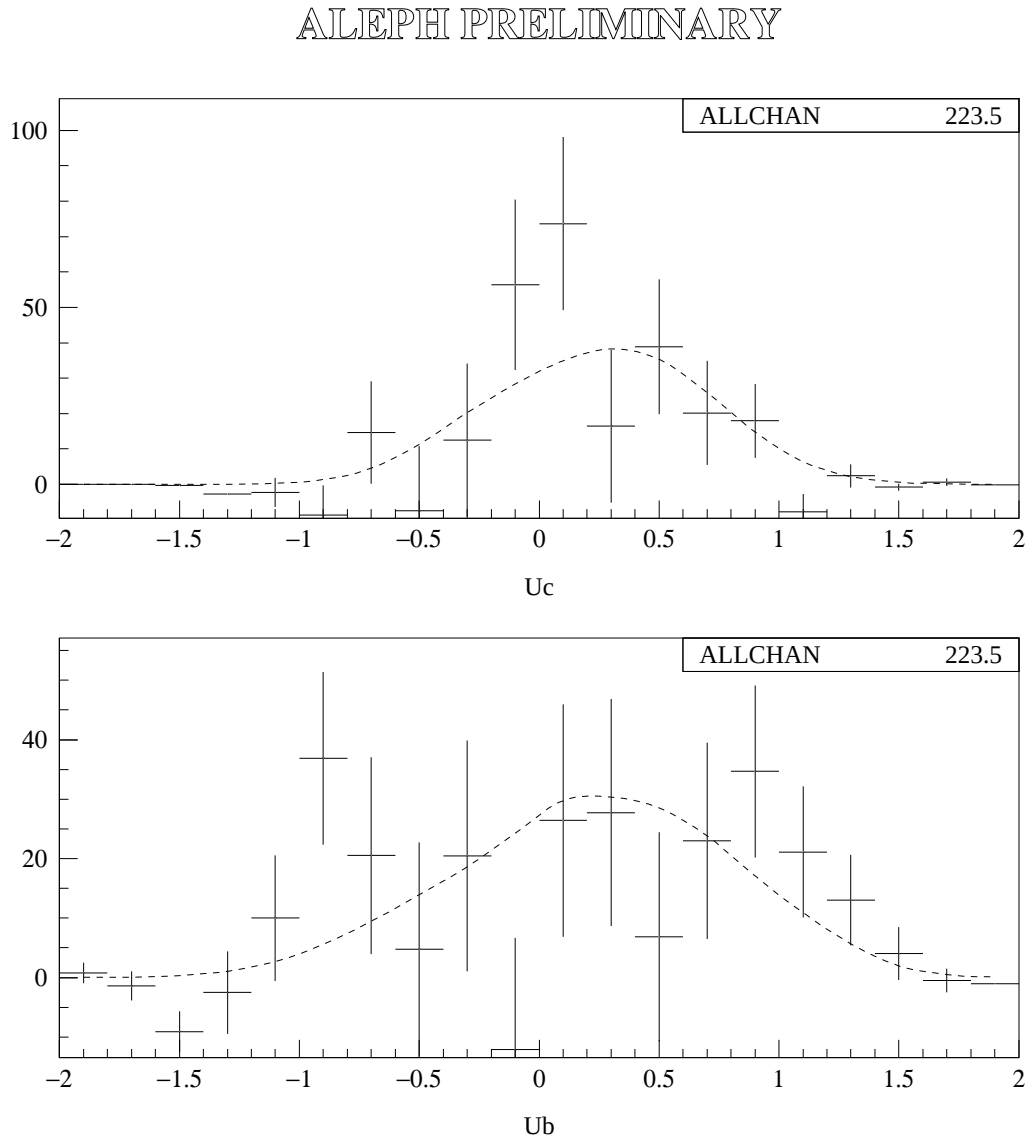

Figure 4: $D_s \rightarrow \tau\nu$ analysis: projections of the two-dimensional fit to the data with backgrounds subtracted, electron channel. The top plot is the U_c projection and the bottom plot the U_b projection. The crosses show the data distribution; the dashed curve is the fitted signal distribution.

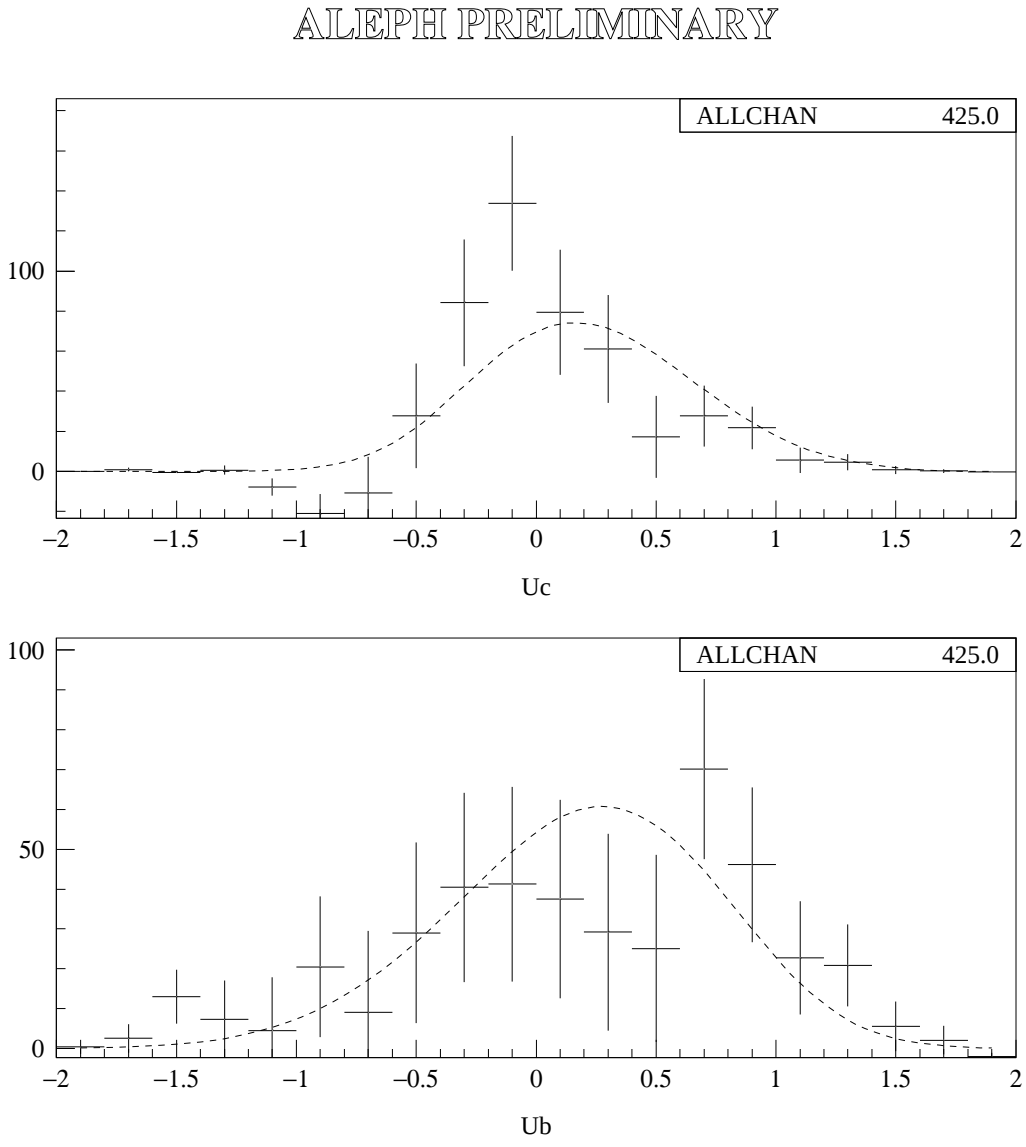

Figure 5: $D_s \to \tau\nu$ analysis: projections of the two-dimensional fit to the data with backgrounds subtracted, muon channel. The top plot is the U_c projection and the bottom plot the U_b projection. The crosses show the data distribution; the dashed curve is the fitted signal distribution.

Table 2: Summary of systematic errors in the $D_s \to \tau\nu$ analysis.

	Relative uncertainty (%)	
Error source	e channel	μ channel
c fragmentation	24.5	21.6
b fragmentation	11.6	12.2
ℓ spectrum in $b \to \ell, b \to c \to \ell, c \to \ell$	19.0	14.7
Charm hadron production in $c\bar{c}$	6.8	3.9
Charm hadron production in $b\bar{b}$	10.3	7.1
Simulation of detector resolution	14.6	11.5
Monte Carlo statistics	16.0	8.8
f_{D_s}/f_D	1.4	2.3
$B(D_s \to \phi\pi)$	32.9	28.2
Total	41.5 ± 32.9[BR]	33.4 ± 28.2[BR]

match the c and b fragmentation parameters recommended in [3]; the mean c and b hadron energies are varied within their uncertainties to evaluate the systematic error on $B(D_s \to \tau\nu)$. The semileptonic decay models generated by OPAL [8] are used to study the uncertainties from the simulation of the lepton momentum spectrum from semileptonic decays of heavy hadrons. The uncertainties from $b \to \ell$, $b \to c \to \ell$, and $c \to \ell$ are combined in quadrature. The uncertainties related to the charmed hadron production fractions in [3–5] are also taken into account.

The resolution on the total reconstructed momentum and energy in $q\bar{q}$ events is found to agree within 5% between real and simulated events. The effect on the measured $B(D_s \to \tau\nu)$ is evaluated by smearing the energies of all neutral particles to yield a 5% degradation in resolution in a sample of simulated signal and background events. The Monte Carlo statistical uncertainties and the theoretical uncertainty on f_{D_s}/f_D are included in the systematic uncertainty on $B(D_s \to \tau\nu)$.

Finally, the results depend on the value of $B(D_s \to \phi\pi)$ assumed in [3–5] because this value affects the number of produced D_s mesons as well as the shapes of the background distributions. The assumed value is $B(D_s \to \phi\pi) = 3.6 \pm 0.9\%$. The corresponding uncertainty on $B(D_s \to \tau\nu)$ is separated from the other systematic uncertainties in the presentation of the final results.

The results from the e and μ channels are combined according to the procedure of [9], taking into account the correlations in the systematic errors. The result is

$$B(D_s \to \tau\nu) = [4.9 \pm 0.9(\text{stat}) \pm 1.6(\text{syst}) \pm 1.4(\text{BR})]\% \ .$$

3 $D_s \to \mu\nu$ analysis

This measurement of $B(D_s \to \mu\nu)$ was first presented in [10].

3.1 Event selection

The selection is optimized to select $e^+e^- \to c\bar{c}$ events containing the decay $D_s \to \mu\nu$. The preselection of hadronic Z decays is performed according to the standard ALEPH selection based on charged tracks. The cut on the number of reconstructed charged tracks coming from the area of the interaction point is tightened to reduce the background from $e^+e^- \to \tau^+\tau^-$ events. The event thrust axis is required to satisfy $|\cos\theta_{\rm thrust}| < 0.8$ to select events within the acceptance of the vertex detector. A loose muon identification algorithm based on muon chamber hits and the digital pattern information from the hadron calorimeter is used to select muon candidates.

A kinematic fit is then performed in order to improve the resolution on the missing momentum, assumed to arise from the undetected neutrino from $D_s \to \mu\nu$. In this fit, the missing mass is constrained to be zero and the D_s displacement direction (from the primary event vertex to some point on the muon track) is constrained to be parallel to the D_s momentum direction. The energies of the reconstructed charged and neutral particles are varied in the fit, while their directions are held constant. The event primary vertex and the D_s decay vertex are also allowed to vary within their uncertainties. The fitted energy of the D_s candidate (the muon and the neutrino) is required to be greater than 15 GeV.

The $b\bar{b}$ background and some of the $c\bar{c}$ background are further reduced by applying the same techniques as in the $D_s \to \tau\nu$ analysis.

Finally, to distinguish signal from the remaining primarily $c\bar{c}$ and $b\bar{b}$ background events a hard cut is made on the energy of the fitted D_s candidate (>25 GeV). The leptonic branching fractions are extracted by means of a fitting procedure which is designed to distinguish between the two principal background components separately. Two linear discriminant variables are created. One is constructed specifically to separate $c\bar{c} \to D_s \to \mu\nu$ events from $b\bar{b}$ background events (mainly containing semileptonic b and c decays), and another to separate them from $c\bar{c}$ background events (mainly containing semileptonic c decays). The linear discriminant variables U_b and U_c are linear combinations of variables which optimally distinguish between two distributions. Each linear discriminant variable is a linear combination of fifteen variables. Plots of the distributions for the $c\bar{c} \to D_s \to \mu\nu$ events and the respective background events are shown in Fig. 6.

The procedure to fit for the $D_s \to \mu\nu$ (plus $D_s \to \tau\nu$) component in the data consists of fitting slices of the invariant mass distribution of the μ and ν combination in 36 bins (6×6) in the (U_b, U_c) plane simultaneously. Fitting functions are generated by separately fitting the mass distributions for each event type in each slice. One to three Gaussians are used depending on the number of events in the slice. The fits for each event type are normalized to one another according to the Monte Carlo predictions. In the fit to the data the backgrounds are divided into two categories, $b\bar{b}$ events and all other events (including $udsc$ events and the few remaining $e^+e^- \to \tau^+\tau^-$ events). The normalization of each background component is allowed to vary separately, while the shapes are fixed. The signal distribution combines the purely leptonic D_s decays from $c\bar{c}$ and $b\bar{b}$ events; it includes a small fraction from $D^+ \to \mu\nu$ and $D^+ \to \tau\nu$ which are nearly indistinguishable from D_s leptonic decays. The constraint $B(D_s \to \tau\nu)/B(D_s \to \mu\nu) = 9.75$ (from Eq. 1) is imposed.

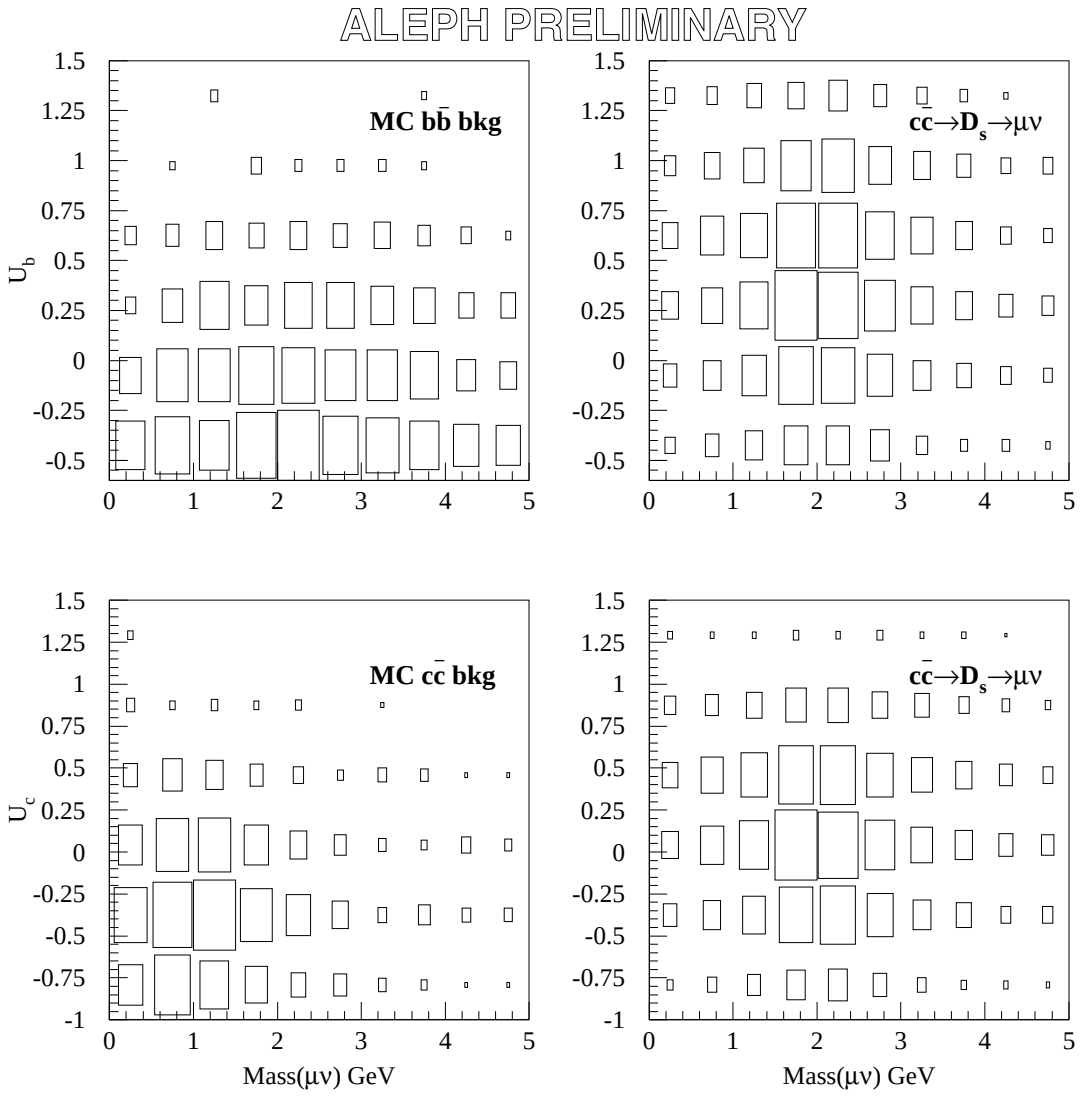

Figure 6: $D_s \to \mu\nu$ analysis: unnormalized U_b vs $M(\mu\nu)$ (top) and U_c vs $M(\mu\nu)$ (bottom) distributions for $b\bar{b}$ background (left) and $c\bar{c} \to D_s \to \mu\nu$ (right), and $c\bar{c}$ background and $c\bar{c} \to D_s \to \mu\nu$, respectively. The same cuts used in the fitting procedure are applied here.

Table 3: Fitted numbers of events in the $D_s \to \mu\nu$ analysis in the individual signal and background components.

Source	No. Events
Signal:	
$c\bar{c} \to D_s \to \mu\nu$	185
$c\bar{c} \to D_s \to \tau\nu$	386
$b\bar{b} \to D_s \to \mu\nu$	108
$b\bar{b} \to D_s \to \tau\nu$	23
$D^+ \to \ell\nu$	46
Total	747
Background:	
uds	593
$c\bar{c}$	2864
$b\bar{b}$	2024
$\tau^+\tau^-$	15
Total	5496

3.2 Results of the $D_s \to \mu\nu$ analysis

The fit to the data, summed over all 36 slices, is shown in Fig. 7. Figure 8 shows the data plus the fitted composition of Monte Carlo events for each of four regions in the (U_b, U_c) plane.

The fitted branching fraction is $B(D_s \to \mu\nu) = [0.670 \pm 0.083(\text{stat})]\%$. The fitted number of signal events is 747 ± 93, while the total number of background events is 5496. The individual contributions are shown in Table 3.

3.3 Systematic uncertainties

There is a small bias in the fitting procedure when run on Monte Carlo events. The fitted signal amplitude is overestimated by a factor of 1.048. The fractional uncertainty due to the limited Monte Carlo statistics is 0.087.

The production fractions of charmed mesons in $b\bar{b}$ and $c\bar{c}$ events are renormalized according to the most recent ALEPH measurements. Applying the corrections to the Monte Carlo distributions produces a shift in the fitted leptonic branching fraction. The production fractions are also varied according to their experimental uncertainties. The sum in quadrature of the variations in the resulting branching fraction measurement plus half the shift is taken as the uncertainty on the branching fraction measurement.

The uncertainty in the signal efficiency due to the muon identification efficiency and the uncertainty on the fragmentation parameter for the signal events is estimated. The muon efficiency is reduced by 20% in the Monte Carlo for muons with $P < 3\,\text{GeV}$ and the data is refitted. The uncertainty due to fragmentation is estimated by lowering the energy cut on the D_s candidate by 2%. The resulting change in the fraction of signal events predicted by Monte Carlo is taken as the uncertainty.

A check on the assumed $\tau\nu/\mu\nu$ signal ratio is done by allowing the $\tau\nu$ and $\mu\nu$ branching

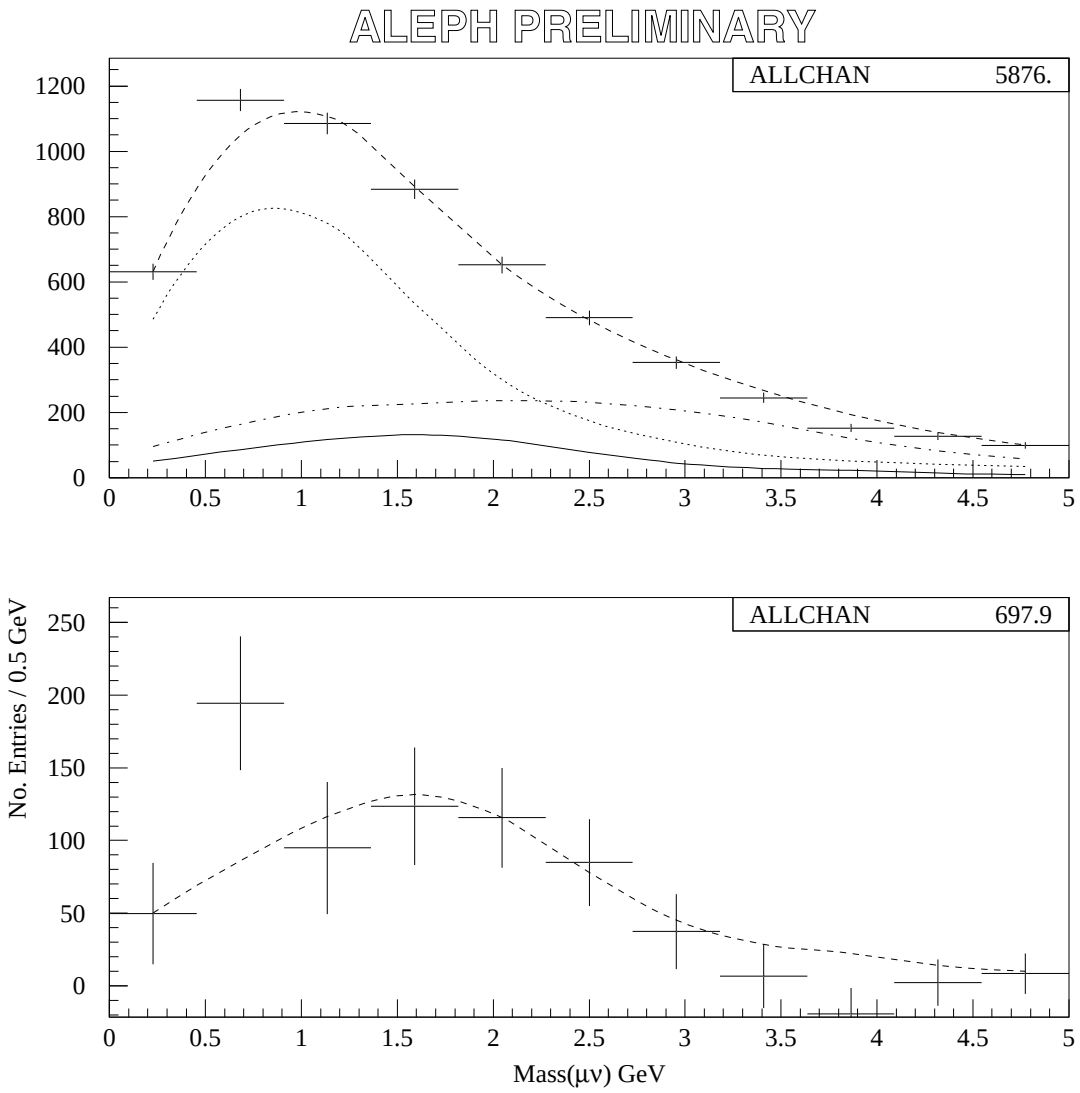

Figure 7: $D_s \to \mu\nu$ analysis: the fit to the mass distribution in the data summed over all 36 slices. The crosses are the data. The top plot shows the data and the fitted contributions. The dashed curve is the sum of all contributions. The dot-dash curve shows the $b\bar{b}$ background events. The dotted curve is the $udsc$ background. The solid curve is the signal. The bottom plot shows the data minus the background, and the curve is the fitted signal contribution.

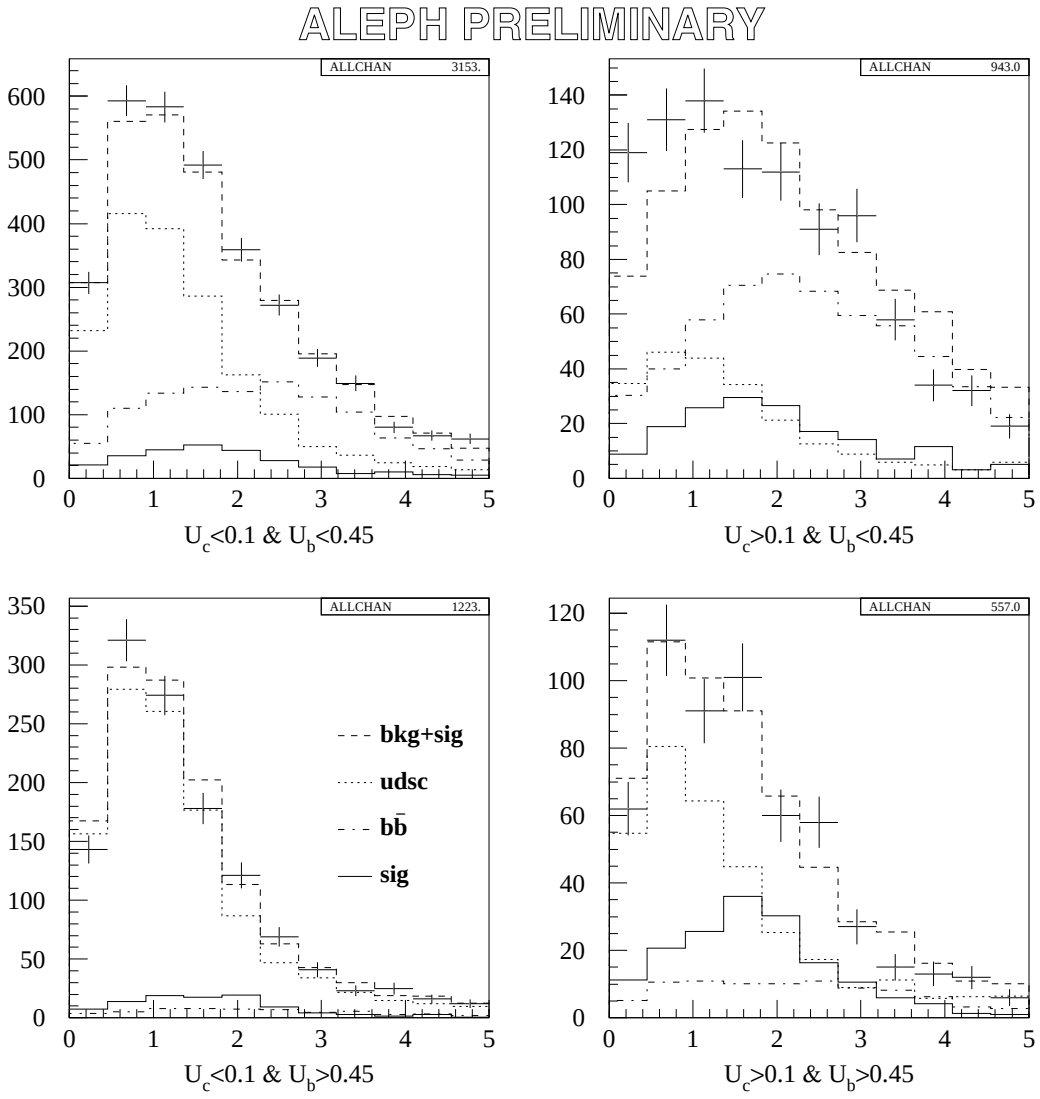

Figure 8: $D_s \to \mu\nu$ analysis: $M(\mu\nu)$ distributions for four regions in the (U_b, U_c) plane. The histograms are the fitted contributions from $udsc$ background, $b\bar{b}$ background, and signal events.

Table 4: Summary of systematic errors in the $D_s \to \mu\nu$ analysis.

Source	Relative uncertainty (%)
Fit bias $\pm$ MC statistics	$+4.8 \pm 8.7$
Hadron production fractions:	
$\Delta/2$	3.2
σ	± 5.6
Physics parameters:	
$f(c \to D_s)$	$\pm 13.3 \pm 19.5$ (BR)
$f(c \to D^+)$	± 0.5
$f(b \to D_s)$	$\pm 1.9 \pm 4.1$ (BR)
$f(b \to D^+)$	± 0.1
$B(D^+ \to \mu\nu)/B(D_s \to \mu\nu)$	± 0.3
$B(D^+ \to \tau\nu)/B(D_s \to \mu\nu)$	± 0.2
Signal efficiency:	
μ identification	± 1
Fragmentation	± 4
Background shape:	
($\sim 5\times$ hadron prod unc)	± 30
Total bias and uncertainty	$+5 \pm 34 \pm 24$ (BR)

fractions to vary independently. The results of this fit are $B(D_s \to \mu\nu) = (0.596 \pm 0.246)\%$ and $B(D_s \to \tau\nu)/B(D_s \to \mu\nu) = 11.8 \pm 7.0$, consistent with the branching fraction fitted above and with the expected $\tau\nu/\mu\nu$ ratio of 9.75.

There remain other significant systematic errors to estimate. The fragmentation parametrization needs to be varied. The composition and properties of the principal background components need to be understood. The reason for the bias in the fitting routine needs to be understood. The effect of detector resolution on the results must be examined.

Table 4 summarizes the systematic uncertainties which have been estimated. The uncertainties under the heading physics parameters refer to uncertainties on the signal. The largest component comes from $f(c \to D_s)$ which almost corresponds to the overall normalization of the signal, since the contributions from the $b\bar{b} \to D_s \to \mu\nu$ and $D^+ \to \ell\nu$ channels are small. The errors labelled (BR) refer to the uncertainty in the measurement of $D_s \to \phi\pi$. The background shape uncertainty is a conservative estimate which includes as yet unaccounted for effects relating to the shape of the background distributions.

4 Conclusions

Preliminary measurements of $B(D_s \to \tau\nu)$ and $B(D_s \to \mu\nu)$ have been made. The results are

$$\begin{aligned} B(D_s \to \tau\nu) &= [4.9 \pm 0.9(\text{stat}) \pm 1.6(\text{syst}) \pm 1.4(\text{BR})]\% \\ B(D_s \to \mu\nu) &= [0.64 \pm 0.08(\text{stat}) \pm 0.21(\text{syst}) \pm 0.15(\text{BR})]\% \ , \end{aligned}$$

where the last error in each case is due to the uncertainty on $B(D_s \to \phi\pi)$.

The results from the two decay channels of the $D_s \to \tau\nu$ analysis and that from the $D_s \to \mu\nu$ analysis are used to evaluate the D_s decay constant within the Standard Model (Eq. 1). The three values are combined, taking into account the correlations in the statistical and systematic errors. The combined result is

$$f_{D_s} = [261 \pm 20(\text{stat}) \pm 43(\text{syst}) \pm 35(\text{BR})]\,\text{MeV} \ ,$$

with a χ^2 of 1.33 for two degrees of freedom (CL = 0.51). This value of f_{D_s} is consistent with previous measurements [7].

References

[1] ALEPH Collaboration, Nucl. Instrum. Methods A346 (1994) 461.

[2] ALEPH Collaboration, Phys. Lett. B313 (1993) 535.

[3] LEP Heavy Flavour Working Group, preprint LEPHF/98-01 (1998).

[4] ALEPH Collaboration, Phys. Lett. B388 (1996) 648.

[5] ALEPH Collaboration, Eur. Phys. J. C4 (1998) 387.

[6] J. Flynn and C. Sachrajda, Heavy Flavours II, edited by A. Buras and M. Linder, World Scientific, Singapore (1998) 402.

[7] C. Caso et al. (Particle Data Group), Eur. Phys. J. C3 (1998) 1.

[8] LEP Heavy Flavour Working Group, preprint LEPHF/94-001 (1994).

[9] L. Lyons, D. Gibaut, and P. Clifford, Nucl. Instrum. Methods A270 (1988) 110.

[10] "Leptonic decays of the D_s meson", ALEPH Collaboration, contributed paper #937 to the XXIX International Conference on High Energy Physics, Vancouver, B.C., 23–29 July 1998.